

Reinterpreting the puzzling properties of $z>6$ galaxies within a variable IMF framework.

Fabio Fontanot^{1,2,*}, Gabriella De Lucia^{1,2}, Lizhi Xie³, Stefano Zibetti⁴, Francesco La Barbera⁵, Sebastiano Cantarella^{6,1}, Michaela Hirschmann^{7,1}, Stéphane Charlot⁸ and Gustavo Bruzual⁹

¹ INAF - Astronomical Observatory of Trieste, via G.B. Tiepolo 11, I-34143 Trieste, Italy

² IFPU - Institute for Fundamental Physics of the Universe, via Beirut 2, 34151, Trieste, Italy

³ Tianjin Normal University, Binshuixidao 393, 300387, Tianjin, People's Republic of China

⁴ INAF-Osservatorio Astrofisico di Arcetri, Largo Enrico Fermi 5, I-50125 Firenze, Italy

⁵ INAF - Astronomical Observatory of Capodimonte, Sal. Moiariello, 16, 80131 Napoli, Italy

⁶ Astronomy Section, Department of Physics, University of Trieste, via G.B. Tiepolo 11, I-34143, Trieste, Italy

⁷ Institute for Physics, Laboratory for Galaxy Evolution, Observatoire de Sauverny, Chemin Pegasi 51, 1290 Versoix, Switzerland

⁸ Sorbonne Université, CNRS, UMR 7095, Institut d'Astrophysique de Paris, 98 bis bd Arago, 75014 Paris, France

⁹ Instituto de Radioastronomía y Astrofísica, UNAM, Campus Morelia, C.P. 58089, Morelia, México

Received ???, 2026; accepted ???, 2026

ABSTRACT

Recent results from the James Webb Space Telescope (JWST) report space densities for bright and massive galaxies at $z>7$ that far exceed expectations of theoretical models of galaxy formation, prompting a revision of our understanding of the physical processes leading to the assembly of the first luminous structures. In this work we present predictions from a realization of the GALaxy Evolution and Assembly (GAEA) model, which implements a prescription for a variable stellar initial mass function (IMF). This prescription is inspired by high-resolution numerical simulations that account for the role of cosmic rays (CR) as regulators of the star formation rate (SFR) in giant molecular clouds. In our approach, SFR density is assumed to be a proxy for the CR density, providing a link between the IMF shape and the predicted physical conditions of the star forming interstellar medium. Our results show that, in our model framework, assuming such a variable IMF reproduces several properties of the $z>6$ galaxy population, with no further modification of the feedback model, including their UV luminosity functions up to $z\sim 13$. In order to compare model predictions with available estimates for the galaxy stellar mass function (GSMF), we reconstruct stellar masses from the model's synthetic photometry assuming a universal IMF, reflecting standard observational practice. Under this approach, we show that the model can reproduce the evolution of the GSMF up to the highest redshifts accessible. Our findings highlight the need to consider a variable IMF shape in the error budget associated with stellar mass estimates. We show that the evolution of both the slope and normalization of the gas-phase mass metallicity relation can be used as powerful discriminant between models of early galaxy formation assuming different IMF evolution.

Key words. galaxies: formation – galaxies: evolution – galaxies: star formation – galaxies: statistics – galaxies: stellar content

1. Introduction

In recent years, the wealth of data coming from the James Webb Space Telescope (JWST) opened new challenges in our understanding of the processes leading to the early formation and assembly of galactic structures at $z \gtrsim 8-9$. The first puzzling evidence came from the discovery of a large population of UV-bright galaxies at such redshifts, now accessible thanks to the observed frame IR capabilities of JWST (see e.g. Robertson 2022). Indeed, derived number densities for this population (Pérez-González et al. 2023; Castellano et al. 2023; Donnan et al. 2023; Harikane et al. 2023a; Leung et al. 2023; Donnan et al. 2024; Harikane et al. 2024; McLeod et al. 2024; Adams et al. 2024; Casey et al. 2024; Finkelstein et al. 2024; Kokorev et al. 2025; Whitler et al. 2025) far exceeded expected UV luminosity function (UVLF) from earlier generation theoretical models of galaxy formation. Despite some of the photometric candidates turned out to be lower-redshift interlopers (see e.g. Arrabal Haro et al. 2023), the number of spectroscopically confirmed bright $z \gtrsim 10$ sources has grown at in-

creasing rate (Carniani et al. 2024; Harikane et al. 2024, among the others). Moreover, attempts to use the available spectrophotometric data to infer the physical properties of these galaxies, through standard SED-fitting approaches led to speculations that also their galaxy stellar mass function (GSMF, see e.g. Navarro-Carrera et al. 2024; Weibel et al. 2024; Shuntov et al. 2025; Harvey et al. 2025) provides critical tension with predictions of theoretical galaxy formation models. Despite the fact that early suggestions of a tension with the standard Λ CDM cosmological model (Labbé et al. 2023) have been recently toned down (see e.g. Yung et al. 2025), relevant discrepancies with the predictions of theoretical models of galaxy formation have been consistently reported (Finkelstein et al. 2024; Yung et al. 2024; Cantarella et al. 2025, among the others). It is important to keep in mind that most of these models have been calibrated to reproduce the properties of galaxies at lower redshifts (typically $z \lesssim 4$), using prescriptions to regulate the key physical mechanism that are also based on observations of the low- z Universe. Therefore their struggles to reproduce the properties of higher redshift progenitors can be ascribed to either an oversimplification of these prescriptions, which are no longer adequate to treat

* e-mail:fabio.fontanot@inaf.it

the different physical properties (in terms of gas content, metallicity) of high redshift galaxies, or to the lack of focus on some physical ingredients that are important at early epochs (see e.g. [Maio & Péroux 2026](#)).

Several explanations have been proposed to explain the tension between theoretical predictions and the observed UVLF and GSMF at $z \gtrsim 7-8$. From the observational point of view, the estimated relevant number of Active Galactic Nuclei (AGN) in the high- z Universe ([Harikane et al. 2023b](#); [Maiolino et al. 2024](#)), like the so-called Little Red Dot population ([Matthee et al. 2024](#); [Kocevski et al. 2025](#); [Akins et al. 2025](#)) suggest that AGN contamination may play a role in boosting the UV luminosities for composite sources. In addition, the treatment of dust attenuation could also play a role, e.g. if outflows are able to effectively remove dust from the galactic environment ([Fiore et al. 2023](#); [Ziparo et al. 2023](#)). From a purely theoretical point of view, several plausible modifications of the treatment of the baryon cycle at high- z have been proposed, including an enhanced efficiency of star formation and/or inefficient stellar feedback ([Dekel et al. 2023](#); [Li et al. 2024](#); [Cantarella et al. 2025](#)). Moreover, an extremely bursty star formation history in the first galaxies would lead to enhancement of the UV flux, with respect to the expectation of models based on smooth star formation histories ([Gelli et al. 2024](#); [Semenov et al. 2025](#)).

Another possible explanation for the UV luminosities of high- z galaxies could be a variation in the shape of the stellar initial mass function (IMF [Trinca et al. 2024](#); [Yung et al. 2024](#); [Cueto et al. 2024](#); [Hutter et al. 2025](#); [Mauerhofer et al. 2025](#)). Indeed, an IMF with an enhanced fraction of massive stars with respect to the local measurements (hereafter a MW-like IMF like a [Kroupa 2001](#) or [Chabrier 2003](#) IMF), would imply a lower mass-to-light ratio and an enhanced production of UV photons per unit star formation rate. On the other hand, it would also predict a larger fraction of Type II supernovae and a lower fraction of mass locked in long-living stars (per solar mass formed). Moreover, it is important to keep in mind that assuming a variable IMF also implies that current estimates for galaxy physical properties available in the literature have to be revised ([Fontanot et al. 2017](#)), as the universality of the IMF represents a strong prior often used in SED fitting codes.

Evidences for a different shape of the IMF with respect to the one observed in the local neighbourhood have been growing in recent times. In the local Universe, both dynamical, lensing and spectroscopic properties of early-type galaxies (ETGs) show deviations from the hypothesis of a universal MW-like IMF ([Cappellari et al. 2012](#); [van Dokkum & Conroy 2012](#); [Dutton et al. 2012](#); [La Barbera et al. 2013](#)). In particular, dynamical mass-to-light ratios are larger with respect to photometric estimates assuming a universal IMF: this difference has been dubbed α -excess in the literature. Moving to higher redshifts, [Gunawardhana et al. \(2011\)](#) found evidences for a flattening of the high-mass end slope of the IMF at increasing star formation rate (SFR) in the Galaxy And Mass Assembly (GAMA) survey. Moreover, several results for early galaxies also favour a Top-Heavy IMF scenario for JWST sources ([Katz et al. 2022](#); [Cameron et al. 2024](#); [Cullen et al. 2025](#); [Curti et al. 2025](#)).

In our previous work ([Fontanot et al. 2017, 2018a, 2024](#)), we have focused on the impact of several variable IMF scenarios on the dynamical and spectroscopic properties of local ETGs, while also discussing the impact of this hypothesis on their star formation and galaxy assembly history. Our results showed a limited impact on the reconstructed star formation histories of galaxies in different stellar masses ranges. In particular, the trend for shorter star formation timescales in more massive galax-

ies is preserved. In the framework of a variable IMF scenario, the main effect is connected with the interpretation of the local chemical enrichment relations in ETGs. In particular, we showed that, in this framework, the level of α -enhancement and the $[\alpha/\text{Fe}]$ ratios do not trace the SFR timescale, but the maximal level of SFR reached in the past ([Fontanot et al. 2017](#), see also [Tinsley & Larson 1979](#)). Moreover, we showed that a variable IMF can significantly affect stellar masses derived from photometry (M_{\star}^{phot}). These photometric masses may differ from the intrinsic stellar mass predicted by theoretical models, thereby biasing the recovery of the intrinsic galaxy stellar mass function (GSMF) from photometric surveys ([Fontanot 2020](#)). This IMF-driven effect on galaxy observables is expected to be stronger in the early Universe, due to the younger ages of stellar populations and shorter timescales sampled by observations.

The aim of the present work is to explore the effect of a variable IMF scenario on the comparison between theoretical predictions and JWST results, both in the observational space (UVLFs) and in the physical space (GSMF). This paper is organized as follows. In Section 2 we introduce the latest realization of the GAEA model, while in Section 2.2 we discuss the assumed variable IMF scenario adopted in this paper. We then present our results for the predicted UV luminosity function in Section 3.1; while in Section 3.2 we discuss the effect of the variable IMF scenario on the stellar mass estimates for $z > 6$ galaxies and compare with recent GSMF measurements. Finally in Section 4 we discuss the implications of our finding and present our conclusions. All magnitudes quoted in this work have been computed in the AB system ([Oke & Gunn 1983](#)).

2. Theoretical models

2.1. The Galaxy Evolution and Assembly (GAEA) model

In this work, we consider predictions from the latest version of the GALaxy Evolution and Assembly (GAEA) model (see [De Lucia et al. 2024](#), and references therein). GAEA is a semi-analytic model (SAM), designed to follow the growth of galaxy populations in a cosmological volume and across a wide redshift range. These models assume that Dark Matter Haloes (DMHs) represent the natural sites for galaxy formation, using the baryons locked in their potential wells since early cosmic epochs. SAMs start from a statistical description of the evolution of DMHs population defined over a cosmological volume and unfold the complex network of physical mechanisms acting on the baryonic gas numerically solving a system of coupled differential equations. Individual prescriptions typically employ approximated parametrizations (which are usually derived from either empirical, numerical or theoretical arguments) to describe the key dependencies on galaxy physical properties. A critical difference with respect to hydro-simulations lies in the lack of an explicit treatment for gas dynamics: this represents an advantage for SAMs, as it drastically reduces the computational demand of the method, thus allowing for a large flexibility in exploring the effect of individual physical processes on global galaxy evolution over large (cosmological) volume and across a wide redshift range. However, this choice also represents a major limitation for model predictions: in their standard implementation, SAMs are indeed not able to track the spatial distribution of the major baryonic components in the multi-phase gas.

The latest rendition of the GAEA model has been recently presented in [De Lucia et al. \(2024\)](#), see also [Xie et al. 2024](#) and [Fontanot et al. 2025](#)). This version combines several updated prescriptions at the same time, in particular:

- ★ a non-instantaneous model for the chemical enrichment of the inter-stellar medium (ISM) (De Lucia et al. 2014);
- ★ a stellar feedback model based on the results of high-resolution numerical simulations (Hirschmann et al. 2016);
- ★ an AGN feedback scheme based on the modelling of cold gas accretion onto SMBHs (Fontanot et al. 2020);
- ★ an explicit partition of cold gas into atomic and molecular component (Xie et al. 2017);
- ★ a detailed treatment for dynamical processes acting on the gaseous component of satellite galaxies (Xie et al. 2020).

With respect to the realization discussed in De Lucia et al. (2024), we modify the prescription for stellar feedback, following results from Cantarella et al. (2025). In detail, GAEA uses a parametrization proposed by Muratov et al. (2015) using numerical experiments up to $z \sim 4$ and extrapolating the relevant trends to higher redshifts (see Eq. 14 and 15 in Hirschmann et al. 2016). In the present work we assume that at $z \gtrsim 4$, stellar feedback efficiencies are capped at their $z=4$ values. Cantarella et al. (2025) showed that the weaker stellar feedback at $z > 4$ leads to an increase of the normalization of the $z \sim 6$ GSMF, while having little impact on the bright end of the UVLF at $z \gtrsim 10$. We consider this model variant as our reference GAEA realization.

As in previous work, we use as a calibration set the evolution of the GSMF up to $z \sim 3$, the evolution of the AGN LF up to $z \sim 4$ and the local HI and H_2 mass functions. In a series of papers, we compare model predictions against several properties of galaxy populations across a wide range of cosmic epochs. In particular, we conclude that our reference GAEA run is able to correctly reproduce:

- ★ the fractions and space densities of quiescent galaxies up to $z \sim 4$ (De Lucia et al. 2024);
- ★ the emission line properties of different galaxy populations (Euclid Collaboration et al. 2024);
- ★ the clustering properties of galaxy populations as a function of stellar mass, star formation activity, HI content and redshift (Fontanot et al. 2025);
- ★ the low-redshift dwarf galaxy ($M_\star \lesssim 10^9 M_\odot$) quiescent fractions (Meng et al. 2023);
- ★ the decreasing trend of HI and SFR of satellite galaxies in cluster halos (Chen et al. 2024);
- ★ the evolution of the UVLF and of the evolution of the mass-metallicity relation in the redshift range $5 < z < 9$ (Cantarella et al. 2025).

In Cantarella et al. (2025), we also considered predictions for the UVLF and GSMF at redshift $z \gtrsim 9-10$, finding an increasing tension between GAEA expectations and observational measurements. In detail, we showed that this tension cannot be completely reduced by considering the effect of the Eddington bias (at least considering up to 0.5 dex uncertainty in the mass determination), and we discussed alternative theoretical scenarios able to explain the mismatch, such as a weaker stellar feedback or a feedback-free starburst scenarios (Dekel et al. 2023). In the present work, we will explore an alternative scenario, which assumes that the stellar IMF associated with early star formation episodes does not match the functional form derived in the Milky Way (i.e. a Kroupa 2001 or Chabrier 2003 IMF), but it favours the formation of massive stars (i.e. a so-called “top-heavy IMF”).

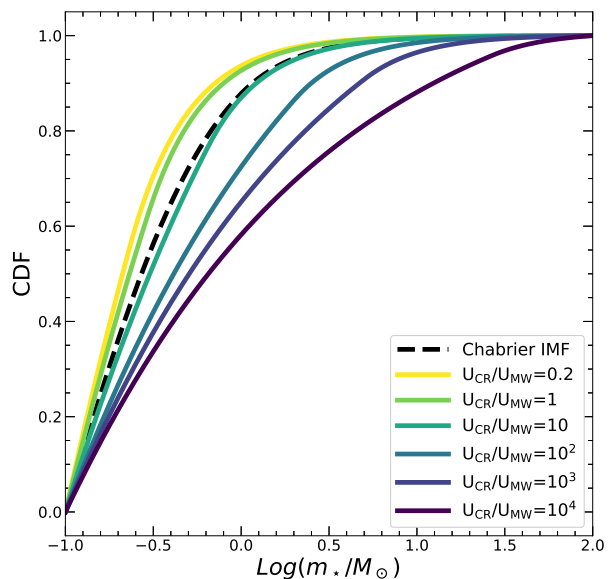


Fig. 1. Cumulative distribution function (CDF) for the different IMFs used in this work. Individual IMF shapes correspond to the IMF library described in Fontanot et al. (2018a), which assumes a dependence of the IMF characteristic stellar mass (i.e. the IMF knee) on the CR density background (U_{CR}), following the numerical simulations of Papadopoulos et al. (2011). At increasing U_{CR} , the characteristic mass get larger, which translates into an increasing the number of massive stars (i.e. a top-heavy IMF - see main text for more details). The black dashed line corresponds to a MW-like IMF, with the shape corresponding to a Chabrier IMF.

2.2. The IMF scenario

In our previous work (Fontanot et al. 2017, 2018a, 2024), we explored the effect of a variable IMF on galaxy properties predicted by GAEA. In particular, we focused on a subset of variable IMF scenarios (Kroupa et al. 2013; Papadopoulos et al. 2011; Weidner et al. 2013; Fontanot et al. 2018b), linking the shape of the galaxy-wide IMF to the global SFR level (or its density) of model galaxies. We showed that these runs correctly reproduce a number of observational properties of low- z galaxies, that are difficult to reconcile with a Universal, MW-like, IMF. One of the critical predictions of the variable IMF framework implies that each star formation episode can be characterized by a different IMF shape, based on the physical properties of the interstellar medium of the host galaxy. This also implies that the IMF varies with both cosmic time and environment.

In this work, we focus on a single model to infer the impact of a variable IMF scenario on the interpretation of high- z observations. Specifically, we adopt the model used in Fontanot et al. (2018a, hereafter F18), which is based on the numerical results of Papadopoulos et al. (2011, PP11 hereafter). This framework assumes that cosmic rays (CRs) associated with stellar evolution (supernovae and stellar winds) can penetrate deeper into the inner cores of molecular clouds (MCs) than UV photons, thereby influencing the ionization and chemical state of star-forming regions. PP11 employed high-resolution simulations to show that the primary effect of varying the CR background (U_{CR} , normalized to the Milky Way value U_{MW}) is the modification of the expected Jeans mass as a function of MC density. F18 used these

numerical results to generate a library of variable IMFs whose shapes scale with the SFR density, assumed here to be a proxy for the CR field. In detail, we assume that the evolution of the IMF shape is mainly driven by changes in its characteristic mass, while the low- and high-mass slopes remain fixed (see, e.g., Fig. 1 in F18). Overall, this implementation leads to an increasingly top-heavy IMF with rising SFR density, corresponding to a larger relative fraction of massive stars per unit stellar mass formed; Fig. 1 shows the cumulative distribution function for the IMFs in the library (the corresponding IMF shapes are shown in Fig. 1 - left panel - in Fontanot et al. 2018a). This choice represents an interesting scenario given the increasing prevalence of compact galaxies and dense starbursts at $z > 6$ in JWST observations (Álvarez-Márquez et al. 2023, 2025).

2.3. Estimating physical properties from synthetic photometry

The main advantage of our approach is that, thanks to the availability of simple stellar population (SSP) models associated with our IMF shapes, we can compute self-consistent broadband photometry for the resulting composite stellar populations and predict both luminosity functions and stellar masses. In particular, we took advantage of simple stellar population synthesis model libraries (Bruzual & Charlot 2003; Vazdekis et al. 2010) built for the IMF shapes we consider. We then use these to construct composite stellar populations combining stars formed with the desired IMFs at different times, and use them to self-consistently predict synthetic spectral energy distributions (SEDs) and broadband photometry, corresponding to our model galaxies.

We use the spectro-photometric information associated to each model galaxy to infer its physical properties, in a similar way to what an observer would have derived¹, assuming a universal MW-like IMF. In order to speed the calculations up while maintaining a classic SED fitting approach, we use the 2-colour method introduced by (Zibetti et al. 2009) to estimate mass-to-light ratios. A comprehensive Monte Carlo library of composite stellar population synthesis models, with a large variety of SFHs and chemical enrichment histories, is used to infer the mass-to-light ratio in the rest-frame i band (M_*/L_i) as a function of the restframe (u-g) and (g-i) colours. This library is bound to include only SFHs consistent with the age of the Universe at $z=6$ and is based on the SSP models produced by the Bruzual & Charlot (2003) spectro-photometric code, assuming a Chabrier IMF. In practice, we bin the models in the 2D (u-g) vs (g-i) colour space and for each bin we consider the median M_*/L_i of the corresponding models. We then estimate photometrically equivalent stellar masses (M_*^{phot}) for each object in our sample starting from its synthetic photometry and extracting the M_*/L_i value from the closest position in this map. For the small sample of sources with colours outside the reference map, we extrapolate a M_*/L_i value via a nearest neighbour approach. We include all relevant details about the generation of the M_*/L_i map in Appendix 4.

2.4. Runs

In the following, we consider prediction draw from the latest GAEA realization presented in Cantarella et al. (2025, see also Fontanot et al. 2025), which couples the model with merger trees extracted from the P-MILLENNIUM simulation (Baugh et al. 2019 – PMS hereafter). The PMS is a DM-only numeri-

¹ In our previous papers we referred to these estimates as “apparent” physical properties (see e.g. Fontanot et al. 2017)

cal simulation defined over a 800^3 Mpc^3 volume and run using the GADGET code (Springel et al. 2005) assuming cosmological parameters consistent with the first year results from the Planck satellite (Planck Collaboration XVI 2014 – $\Omega_\Lambda = 0.693$, $\Omega_m = 0.307$, $\Omega_b = 0.04825$, $n = 0.9611$, $\sigma_8 = 0.8288$, $H_0 = 67.77 \text{ km/s/Mpc}$). The particle mass resolution is $1.06 \times 10^8 h^{-1} M_\odot$ and merger trees have been constructed starting from DMHs resolved with at least 20 particles, over a grid of 128 snapshots, equally spaced in expansion factor². This implies that GAEA reliably models galaxies down to a stellar mass limit of $\sim 10^8 M_\odot$. In Fontanot et al. (2025) we showed that GAEA predictions are consistent for runs over other cosmological simulations belonging to the same suite, assuming different Λ CDM parameters (i.e. the MILLENNIUM and MILLENNIUM-II simulations), that have been used in our previous work.

In the following we consider predictions from two separate GAEA realizations. A first one corresponds to our standard run, assuming a universal IMF in the form proposed by Chabrier (2003). We then run a new model, implementing the variable IMF described in F18 and keeping the same model parameters as in the standard run. As in F18, we assume that the SFR surface density (Σ_{SFR}), computed using the disk radius (3.2 times the exponential scale length of the gaseous component), is a good proxy for U_{CR} , such as:

$$\frac{U_{\text{CR}}}{U_{\text{MW}}} = \frac{\Sigma_{\text{SFR}}}{\Sigma_{\text{MW}}} \quad (1)$$

where $\Sigma_{\text{MW}} = 10^{-3} M_\odot \text{ yr}^{-1} \text{ kpc}^{-2}$, represents the reference value for the MW disc. We do not attempt to recalibrate³ the run with a variable IMF to best reproduce the available information on the evolution of the UVLF, which can be then considered a direct predictions of our framework, highlighting the impact of a variable IMF hypothesis on the predicted photometric and physical properties of model galaxies. For both realizations, we saved the physical properties for all galaxies in the PMS volume, plus we compute the observed-frame photometry in each of the 8 JWST NIRcam wide filters, the restframe UV luminosity using a top-hat filter centred at 160 nm and 20 nm wide and the restframe optical photometry in the ugi-SDSS filters.

3. Results

3.1. Luminosity Functions

We first focus on the predicted galaxy UVLFs from our GAEA realizations. In Fig. 2, we compare the predictions from our standard run (i.e. Cantarella et al. 2025, black dashed line), with the run with a variable IMF (red solid line). In both cases we show predictions corresponding to unattenuated magnitudes, i.e we are not considering the effect of dust. This choice is driven by the consideration that the standard treatment for dust attenuation in GAEA, is based on a simple model calibrated to low- z observations (Charlot & Fall 2000), and might not represent an ideal framework to model dust attenuation at higher redshifts. Moreover, Cantarella et al. (2025) showed that the GAEA unattenuated UVLFs are in better agreement with observations at $z \gtrsim 7-8$. In

² This correspond to roughly half of the available snapshots in the PMS. This choice help reducing the computational load and output size of the model, without affecting the results as shown in (Cantarella et al. 2025).

³ The model realization considered in F18 and calibrated on low- z LFs was based on an earlier version of the GAEA model.

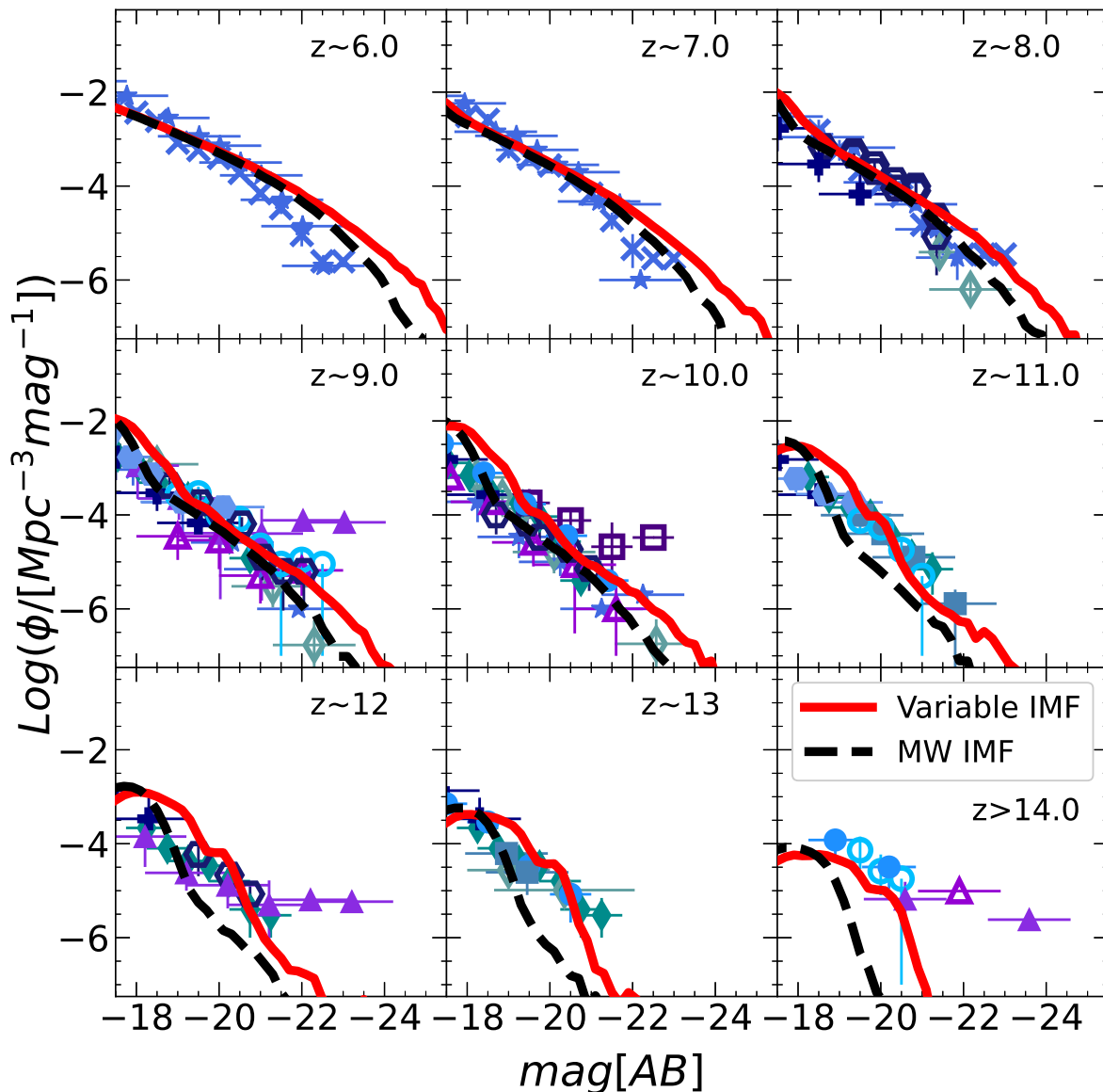


Fig. 2. Redshift Evolution of the UV Luminosity Function at $z > 6$. Black dashed and red solid lines correspond to the predictions of the *GAEA* realization assuming a universal MW-like IMF and the variable IMF scenario from Sec. 2.2. Observational datapoints from Finkelstein et al. (2015, crosses), Bouwens et al. (2021, stars), Pérez-González et al. (2023, pluses), Castellano et al. (2023, empty squares), Donnan et al. (2023, empty diamonds), Harikane et al. (2023a, empty triangles), Leung et al. (2023, filled hexagons), Donnan et al. (2024, filled diamonds), Harikane et al. (2024, filled triangles), McLeod et al. (2024, filled squares), Finkelstein et al. (2024, empty circles), Adams et al. (2024, empty hexagons), Whitler et al. (2025, filled circles).

a forthcoming paper, we plan to better characterize the impact of dust extinction in *GAEA*, by including an explicit modelling for the growth and destruction of dust grains (Osman et al. 2025).

Overall, the variable IMF scenario leads to an increase of the space density of UV sources at all magnitudes above the resolution of the model. The effect is larger at increasing redshifts, which is a consequence of the larger contribution of top-heavy IMFs: in detail, the variable IMF run predictions (red lines) are consistent with most of the observed LFs and they converge to

the standard run predictions at $z \lesssim 7$ (black dashed lines). This convergence in the predictions at decreasing redshift suggests a dominant role of compact star forming galaxies at high- z , corresponding to a larger contribution of stellar populations associated with a top-heavy IMF. This is clearly shown in Fig. 3, that displays the predicted U_{CR}/U_{MW} distribution for our model galaxies at different redshifts. There is a clear evolution of the peak of the distribution with redshift, which reflects in a shift of the typical IMF associated with star forming galaxies at differ-

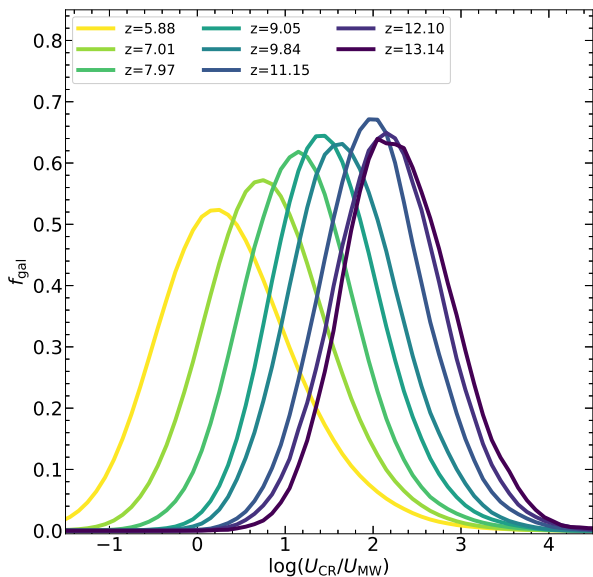


Fig. 3. Predicted $U_{\text{CR}}/U_{\text{MW}}$ distribution for GAEA model galaxies in the variable IMF realization. Different redshift are shown in different colours as in the legend.

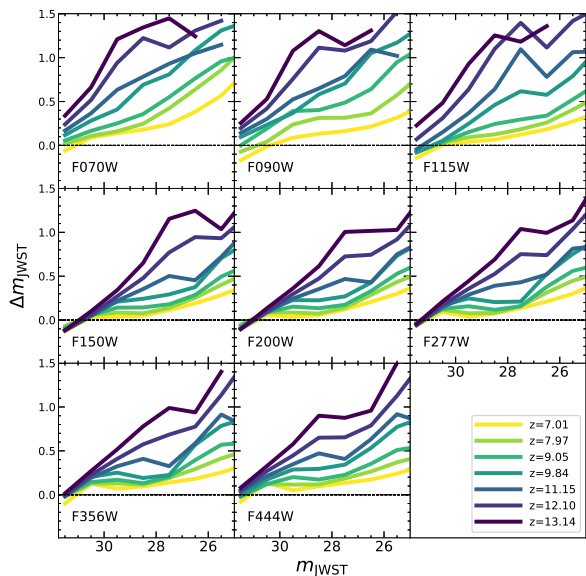


Fig. 4. Photometric differences in JWST filters between a GAEA realization assuming a universal MW-like IMF and the run with the variable IMF. Each panel shows results for a given JWST wide filter (indicated in the label), predictions at different redshifts are marked by a different colour as in the legend.

ent redshifts. Higher-redshift sources tend to be characterized by top-heavier IMFs in the PP11 variable IMF GAEA realization.

In our approach, different IMF shape are associated with different SSP libraries. We use this information to generate synthetic photometry for each model galaxy, that self-consistently takes into account the IMF variations along the its formation

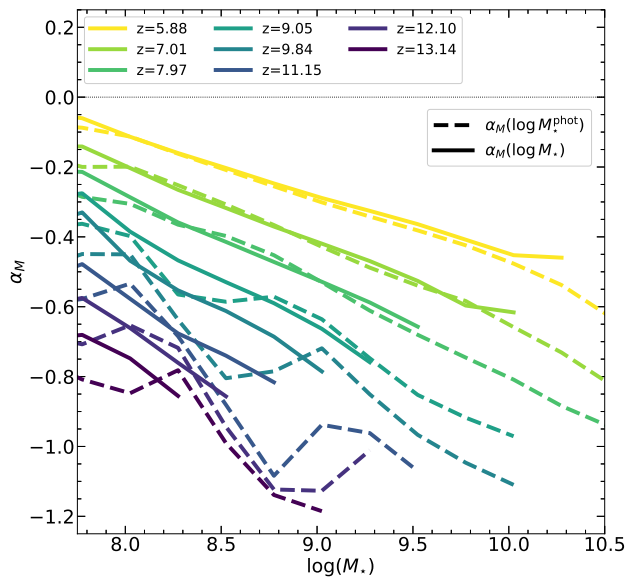


Fig. 5. Logarithmic Mass difference α_M between the intrinsic stellar mass in the variable IMF run and M_{\star}^{phot} , i.e. the stellar mass reconstructed from synthetic photometry assuming a MW-like IMF. Coloured lines refer to different redshifts as in the legend. Solid and dashed lines refer to the α_M dependence on M_{\star} and M_{\star}^{phot} , respectively. Note that, on average, stellar masses in the variable IMF scenario are lower than those estimated for a MW-like IMF (see the main text for a discussion)

history. For each source in our simulated volume, we can compare the observer-frame magnitudes in the 9 wide JWST filters both for the reference run, assuming a MW-like IMF ($m_{\text{JWST}}^{\text{MW}}$) and in the variable IMF run (m_{JWST}). In Fig. 4, we show the mean difference ($\Delta m_{\text{JWST}} = m_{\text{JWST}}^{\text{MW}} - m_{\text{JWST}}$) between these two predictions. The magnitude difference is not only driven by the different SSPs, but also incorporates the changes in the physical properties of high- z stellar populations, due to the IMF variations, i.e. the returned fraction, the chemical enrichment and the fraction of baryons locked into low-mass stars. Indeed, the star formation histories of individual model galaxies are different between the two runs. In Fig. 4 we show the magnitude difference between the variable-IMF and the standard-IMF predictions as a function of m_{JWST} . Each panel is for a single JWST filter (blue to red, starting from the top left panel), while different lines refer to different redshift (as indicated in the legend). Overall, magnitudes in the variable IMF realization are brighter than the corresponding estimates in a universal IMF run. The difference tend to increase with galaxy luminosity and redshift, consistent with the results from the UVLF analysis. At magnitudes around 30, differences are negligible at most redshift but for the bluest filters, while they can reach up to 1.5 magnitudes at 26 mag for the most extremes IMF variations. These results suggest that IMF variations might offer a plausible theoretical explanation for the extremely luminous sources observed at the highest redshifts, without requiring changes to the star-formation or feedback prescriptions relative to those adopted at lower redshift (see e.g. Cantarella et al. 2025, and references herein). Fig. 4 shows that the variable IMF run goes in the right direction and can account for a large part of the tension between observations and the predictions of the reference model. Next we analyse whether this can provide also a quantitative solution to these tensions.

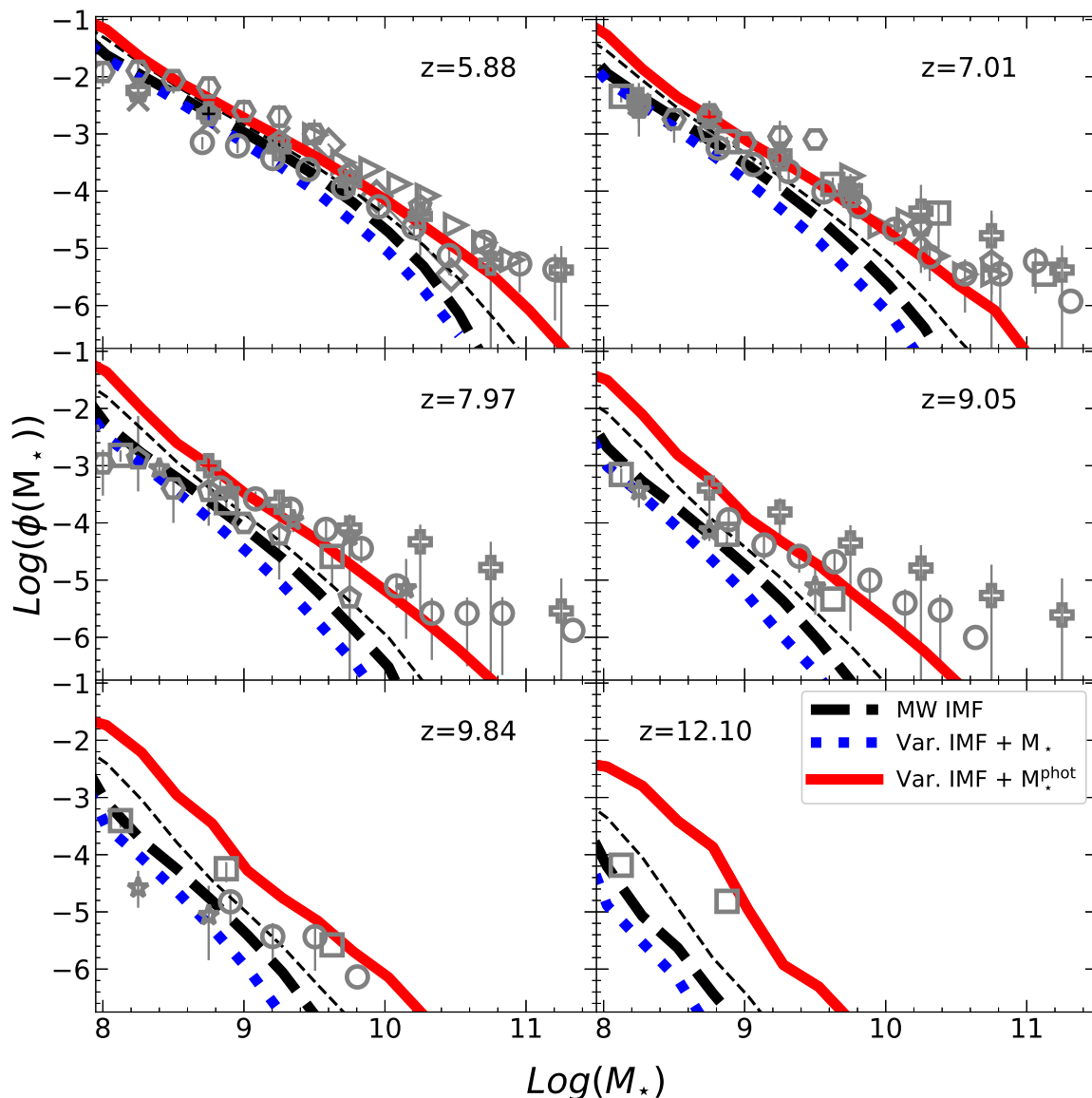


Fig. 6. Evolution of the galaxy stellar mass function at $z > 6$. Dashed black, blue dotted and red solid lines refer to GAEA predictions for the standard - MW-like IMF - run, the variable IMF run using the intrinsic M_* and the variable IMF realization using the photometrically derived M_*^{phot} . Thick and thin lines refer to intrinsic GSMF and to realizations taking the Eddington bias into account (see text for more details). Predictions are compared with data from [González et al. \(2011, crosses\)](#), [Grazian et al. \(2015, triangles\)](#), [Song et al. \(2016, pentagons\)](#), [Stefanon et al. \(2015, diamonds\)](#), [Stefanon et al. \(2021, stars\)](#), [Navarro-Carrera et al. \(2024, hexagons\)](#), [Weibel et al. \(2024, pluses\)](#), [Shuntov et al. \(2025, circles\)](#), [Harvey et al. \(2025, squares\)](#).

3.2. Estimate for stellar masses

Taking advantage of the GAEA coupling with spectro-photometric codes, we can use the self-consistently derived photometry for each of our model galaxies to provide an estimate for the expected stellar masses assuming a MW-like IMF. It is worth stressing that since our code is predicting JWST wide filter magnitudes, it would be possible to run exactly the same pipelines that have been employed in JWST surveys on both realizations.

As we discussed in the introduction, a number of observational results at low-redshifts reported a mismatch between the estimate of the stellar mass of a galaxy derived from dynamical modelling and/or from the analysis of spectroscopic features and the corresponding photometric estimate (obtained through mass-to-light argument or via SED fitting algorithms, assuming a MW-like IMF). This mismatch has been referred to as the α -excess. In our previous theoretical work (starting from [Fontanot et al. 2017](#)), we assumed that the intrinsic stellar mass predicted by

the model correspond to the dynamical stellar mass, while we derived the photometric stellar mass from synthetic photometry. We thus define an α -excess for model galaxies assuming $\alpha_M = \log(M_\star/M_\star^{\text{phot}})$, and we study its dependence on both redshift and stellar mass. Photometric stellar mass estimates can suffer from systematic biases beyond IMF mismatch, particularly from assumptions about the SFH. To quantify these, we compute α_M for galaxies in the MW-like IMF realization — i.e., matching the assumed SSP library IMF. At $6 < z < 8$, photometric estimates recover the intrinsic M_\star to within a few 0.01 dex, but at higher redshifts we find negative α excess reaching ~ 0.2 dex at $z \sim 12$. Two effects drive this. First, the SSP library includes models up to the Universe's age at $z=6$, which exceeds the maximum age at higher redshifts. These models therefore contain larger fractions of low-mass, low-luminosity stars that inflate the mass-to-light ratio. Second, galaxies at higher redshift are likely to have intrinsically burstier SFHs, which tend to have systematically lower mass-to-light ratios than smoother SFHs. As shown by Gallazzi & Bell (2009), broad-band colours alone cannot distinguish SFH types; therefore, the use of an SSP model library not specifically designed to match bursty SFHs leads to systematic M_\star overestimates of up to 0.1–0.2 dex. While confirming that photometric masses may be significantly biased, this test places an upper limit of 0.2 dex on SFH-driven systematics.

In Fig. 5, we show the resulting α -excess for our model galaxies in the variable IMF run. We consider the α_M dependence on both M_\star (solid lines) and M_\star^{phot} (dashed lines). It is quite clear that the absolute value of α_M strongly increases with redshift, thus reflecting the increasing contribution of stellar populations characterized by top-heavy IMFs. Fig. 5 also highlights two important properties of the model galaxy populations in the variable IMF realization. First, the α_M at $z \gtrsim 7$ –12 is both larger than the SFH-driven systematics we already discussed and larger than the claimed typical errors on derived M_\star at these redshifts (i.e. a statistical error of the order of 0.1 dex of the reconstruction, see e.g. Carnall et al. 2023): this result stresses that a variable IMF scenario may have a relevant impact in the interpretation of observed data. Second, at variance with lower-redshifts ETGs (which are characterized by a positive α -excess), the recovered α_M systematically lie at negative values. This is due to the fact that at low- z ETGs have been selected to be passive galaxies dominated by old stellar populations, while our high- z galaxy sample consists of star forming sources dominated by young and intermediate aged stars. The different composition of stellar populations induces the different trends in α_M : indeed, at young ages, the mass and luminosity budget is dominated by massive stars, having a lower M_\star/L_i , while at low redshifts, the mass is dominated by stellar remnants, implying an $\alpha_M > 1$.

These results have a direct impact on the estimated evolution of the GSMF at $z > 6$. In Fig. 6 we compare different theoretical estimates for the GSMF against the available observational determinations (points with errorbars, all derived assuming a MW-like IMF). We consider the GSMFs based on three different estimates for stellar mass: the M_\star predicted from the GAEA run assuming a MW-like IMF (black dashed lines - see also Cantarella et al. 2025); the actual M_\star predicted by the run implementing the variable IMF (blue dotted lines); the M_\star^{phot} derived from our synthetic photometry, assuming a universal IMF to estimate the mass-to-light ratio (red solid lines). Thick lines display the GSMFs based on the models' intrinsic predictions, for all cases. In addition, with thin lines we show the predictions of the GSMFs for the MW-like IMF realization including the effect of the observational errors on M_\star , which we compute by con-

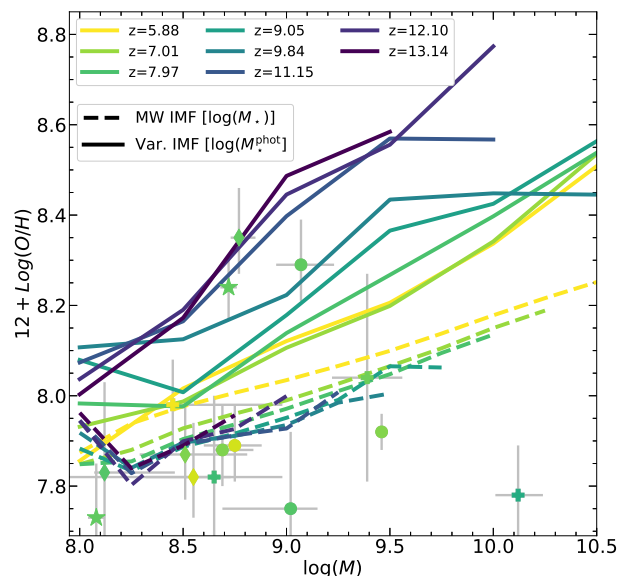


Fig. 7. Evolution of the gas phase mass-metallicity relation at $z > 6$. Dashed lines refer to the predictions for the GAEA realization assuming a MW-like IMF as a function of M_\star , while the solid lines correspond to the metallicities as a function of M_\star^{phot} in the GAEA run implementing the variable IMF. Coloured lines refer to different redshift as in the legend. Datapoints from Nakajima et al. (2023, diamonds), Morishita et al. (2024, circles) and Curti et al. (2024, stars).

volving individual stellar mass estimates with a lognormal error distribution with a 0.25 dex amplitude. In general, we see that by including errors, the agreement of the predictions for this run with the observed datapoints improves, due to the broadening of the GSMF at the high-mass end.

The model assuming a MW-like IMF (black dashed lines) provides a good agreement with the data up to $M_\star < 10^9 M_\odot$ and $z \sim 9$, but it falls short at higher masses and redshifts. GSMFs estimates from the variable IMF GAEA run based on M_\star^{phot} (red solid lines) show larger number densities over the whole stellar mass range, in good agreement with the observational constraints. At lower redshifts, ($6 < z < 9$), GSMFs are closer to the expectations for the run with a MW-like IMF: this is consistent with the results from the F18 model, that shows good agreement between the $z < 3$ GSMFs based on photometric stellar masses and the predictions from GAEA runs based on the universal IMF. It is important to also consider the intrinsic GSMF predictions for the GAEA realization with a variable IMF (blue dotted lines): these systematically lie below the black dashed lines. This is due to the fact that a top-heavy IMF implies less baryons to be locked in long living stars and a larger gas mass fraction to be recycled back into the ICM and IGM to foster subsequent stellar populations. The comparison between the blue dotted and the red solid lines clearly shows the impact of a possible mismatch between the IMF used to estimate physical quantities for high- z sources and their intrinsic IMF when interpreting the properties and evolution of high- z galaxy populations.

3.3. Mass-Metallicity relation

An additional observational signature that is sensitive to the IMF is metallicity. In Fig. 7, we show the redshift evolution of the gas-phase MZR in the GAEA run assuming either universal MW-like IMF (dashed lines) or the variable IMF scenario (solid lines). In order to improve the comparison with observational data, in the former scenario the MZR is shown as a function of M_{\star} , while in the latter as a function of M_{\star}^{phot} . As in our previous work (Fontanot et al. 2021; Cantarella et al. 2025), we consider only model galaxies with a gas fraction larger than 0.1 and we apply a 0.2 downwards shift to the predictions to account for the normalization shift between theoretical predictions and the observed relation at $z < 0.2$. In Cantarella et al. (2025), we showed that model galaxies in our reference run assuming a MW-like IMF are characterized by high gas-phase metallicities: the resulting gas-phase MZR is offset high by ~ 0.3 dex at $3 \leq z \leq 9$, while the predicted slope of the relation is consistent with the best-fit to the data (Morishita et al. 2024). Moreover, the overall MZR is hardly evolving in shape and normalization at $z > 5$.

An interesting prediction of the variable IMF realization is the decreasing normalization of the MZR with redshift (of the order of ~ 0.3 dex from $z \sim 12-13$ to $z \sim 6$), which represent a trend opposite to the reference run with MW-like IMF. In fact, in the standard scenario with a time-invariant universal IMF, the overall metal content is gradually increasing with cosmic time, as the result of subsequent stellar populations, each of them releasing the same metal yield in the ISM. On the other hand the variable IMF run is characterized by top-heavier IMFs, implying larger SNe fraction and larger metal enrichment at higher redshift. As redshift decreases, the metal output from younger stellar populations decreases as well (since they are born within an IMF with a decreasing SN fraction). Moreover, the accretion of gas with pristine composition contributes to the dilution of the overall ISM metallicity. Overall, the variable IMF realization predicts gas-phase metallicities that are in tentative agreement with some sparse JWST results at $z \gtrsim 6$, based on the electron temperature (T_e) method (Nakajima et al. 2023; Curti et al. 2023, 2024; Morishita et al. 2024; Sanders et al. 2024). It is worth stressing, that most of these determinations for high redshift galaxies use strong emission (auroral) line. However, these method have been usually calibrated at lower redshift: therefore they could result in systematic biases when applied to high- z galaxies, due to their different ISM ionization properties (see e.g. Sanders et al. 2023; Curti et al. 2024). Moreover, we are assuming standard yields for short-lived stellar populations (i.e. Chieffi & Limongi 2002), usually calibrated on regular Population II stars. If instead massive stars at the highest redshift are characterized by different yields (e.g. Pop III stars Nomoto et al. 2005), this will likely have an impact on our predictions. We will explore the impact of early Pop III enrichment on the evolution of the MZR in future work (Cantarella et al., in preparation).

3.4. Comparison with other models

The results we present in this section can be compared with the predictions of alternative theoretical models that attempt to implement a variable IMF prescription. Yung et al. (2024) explore the impact of a top-heavy IMF within the framework of the Santa Cruz SAM (Somerville et al. 2015). Their approach does not include a self-consistent implementation of a variable IMF prescription, but it considers the increase in UV luminosity due to the expected increase in the number of massive stars. They show that their model predictions can be reconciled with observational

determinations of the UVLF assuming an increase in UV luminosity by a factor of 4, well within the capabilities of a variable IMF scenario. Our results confirm their suggestion by means of a self-consistent implementation of a variable IMF.

In a recent paper, Somerville et al. (2025) propose a new variant of the Santa Cruz SAM, implementing a density modulated star formation efficiency. In this approach, motivated by results from numerical simulations, star formation efficiency increases as a function of the MCs surface density. Somerville et al. (2025) show that this assumption leads to $z > 9$ space densities up to two orders of magnitude larger than their reference model based on standard Schmidt-Kennicutt prescription, in better agreement with the observational constraints. This model employs a MW-like IMF, nonetheless it is interesting to notice that, in order to reproduce the high- z JWST observations, it resorts to a variation in the SFR prescription based on the gas density. This assumption is conceptually consistent with our approach of changing the IMF shape as a function of SFR density, suggesting gas density as one of the main drivers of galaxy evolution (see also Zibetti & Gallazzi 2022).

The theoretical approach that is closer to ours is probably the one implemented in the DELPHI (Mauerhofer et al. 2025) and ASTREUS (Cueto et al. 2024; Hutter et al. 2025) suites. All these works implement a variable IMF prescription inspired by the numerical results of Chon et al. (2024): starting from a Kroupa functional shape, their IMFs become progressively top-heavier, by assuming a log-flat distribution at the massive end with a slope getting shallower at increasing redshift and decreasing metallicity. They also compute a self-consistent synthetic spectro-photometry for their model galaxies, by using stellar tracks from Starburst99 stellar population synthesis code (Leitherer et al. 1999).

Their results confirm that the assumption of a variable IMF provides a better fit to UVLFs at $z \gtrsim 10$, thanks to the larger fraction of massive stars, leading to brighter sources at fixed SFR. Mauerhofer et al. (2025) also consider the evolution of the GSMF, and they show that a model with a variable IMF implies lower mass-to-light ratios leading to smaller stellar masses at fixed UV luminosity. Their intrinsic GSMFs underpredict the observational constraints at most redshift. However, they do not attempt to infer the stellar masses directly from their synthetic photometry under the assumption of a MW-like IMF, so a direct comparison with literature data is difficult. Both Cueto et al. (2024) and Mauerhofer et al. (2025) also consider the evolution of the high- z gas-phase MZR: they also find an increase in the normalization of the relation at increasing redshift (corresponding to an increase of the top-heaviness of the relation), consistent with our findings. However, the difference between the MZR in their variable IMF scenario, with respect to runs with constant IMF amounts to roughly 0.5 dex at all redshifts, while our model instead predicts a strong redshift evolution of the MZR relation.

It is not easy to identify the physical origin of such different trends. In Mauerhofer et al. (2025) all DELPHI model variants have been independently calibrated to reproduce the $5 < z < 15$ UV-LF by construction, while in our approach we retain the same parameters proposed by Fontanot et al. (2025) to reproduce the GSMF and AGN-LF at $z < 4$. Our choice is further corroborated by the evidence that most predictions from this specific variable IMF model converge to the predictions of the standard run at $z \sim 6$, thus ensuring that the good agreement with the lower redshift galaxy populations is preserved. Moreover, GAEA also include both SMBH accretion and cold gas partition prescriptions, which have been shown to be fundamental to control the baryon cycle and the SFR (De Lucia et al. 2024). A physical mecha-

nisms which is still lacking in the GAEA framework, and most likely of relevance for interpreting the high- z galaxy population is a self-consistent treatment of dust production and destruction. We recently present such an implementation (Osman et al. 2025) and we are planning to exploit it in the context of high- z galaxies and variable IMF scenarios in a future work (Osman et al. in preparation).

4. Summary and conclusions

In this work, we present the predictions of a GAEA model implementing a variable IMF scenario. We assume that the evolution of the IMF is characterized by an increase of the characteristic stellar mass (i.e. the knee of the IMF) at increasing SFR density, inspired by the work of Papadopoulos et al. (2011). We stress that in the original work the IMF variability is driven by the local CR density field, while in this work we assume the SFR density as a proxy for CR density. In this paper, we show that the impact of the variable IMF gets larger at increasing redshift, with larger deviations from the properties predicted by the reference run assuming a MW-like IMF at increasing redshift. This result suggests a scenario where the global CR density field increases with redshift, as a consequence of increasing density and/or specific star formation rate. In our framework, this corresponds to a scenario with an increasingly top-heavier IMFs at increasing redshift. As such, this paper represents an exploratory work to assess the overall impact of the IMF variability on our interpretation of high- z data, in particular from JWST surveys.

Our results show that stellar populations associated with a top-heavier IMF, naturally predict an increase in the rest-frame UV flux, with respect to a universal MW-like IMF scenario, driven by the corresponding larger fraction of massive stars. When compared with available data, our model is thus able to better reproduce the UVLF up to $z \sim 13$. GAEA also predicts that the brightening is not only limited to the UV restframe, but it affects all magnitudes corresponding to JWST wide filters (from F070W to F444W). This effect scales with the magnitude and redshift and it is particularly relevant (~ 1 mag) at the bright end (mag $\lesssim 27$). The larger fraction of massive stars also implies a larger fraction of SNeII and a larger baryon returned fraction. Overall, this implies smaller stellar mass for GAEA model galaxies at fixed UV magnitude, with respect to the standard realization. This corresponds to a negative α -excess (i.e. the ratio between the intrinsic stellar mass and the stellar mass estimated under the assumption of a MW-like IMF - it has been dubbed “excess” since this is typically positive at lower redshifts), and GSMFs based on intrinsic stellar masses that have even smaller space densities than the observational constraints. Nonetheless, it is worth stressing that the model GSMFs for the variable IMF realization built using the photometric stellar mass estimates (i.e. the stellar masses derived from our synthetic photometry assuming a MW-like IMF), are in good agreement with the results from high- z surveys up to $z \sim 12$. The variable IMF scenario leaves also a strong imprint in the chemical enrichment history of model galaxies. In particular it implies a normalization of the gas-phase MZR at $z \gtrsim 6$ larger than available estimates, a steeper relation and a decreasing evolution of the normalization with redshift (at variance with the model using a MW-like IMF).

All those results represent an attempt to self-consistently address the effect of a variable IMF scenario in a galaxy formation model at $z > 6$. Consistently with this approach, we do not attempt any recalibration of GAEA model parameters with respect to the standard run (assuming a Chabrier IMF): this implies that any difference in model predictions is only driven by the IMF varia-

tion. This in turn implies that a more focused work on the variable IMF realization, may also lead to a better agreement with the available data. We advocate that the next step should involve more sophisticated models, self-consistently linking the IMF shape to host high- z galaxy properties (see e.g. Jeřábková et al. 2018; Chon et al. 2024; van Dokkum & Conroy 2024 among the others).

A variable IMF scenario is also entangled with the study of a possible contribution of the so-called Population III stars. In this work, we consider IMF variations that only include Population II stars, i.e. focusing on the relative fraction of stars in different mass ranges. However, Pop III stars are expected to be characterized not only by a different IMF (see e.g. Hirano et al. 2015; Hosokawa et al. 2016), but also by a different dynamical mass range (in most scenarios only massive stars are expected to form, with typical masses much larger than the maximum allowed for standard populations Omukai & Palla 2003). Moreover, their chemical enrichment patterns (i.e. stellar yields) are predicted to be quite different from MW-like populations (see e.g. Nomoto et al. 2005). We leave a more detailed study of the impact of a Population III scenario on the interpretation of high- z observations in a forthcoming work (Cantarella et al., in preparation).

Acknowledgements. An introduction to GAEA, a list of our recent work, as well as datafile containing published model predictions, can be found at <https://sites.google.com/inaf.it/gaea/home>. We acknowledge the use of INAF-OATs computational resources within the framework of the CHIPP project (Taffoni et al. 2020) and the INAF PLEIADI program (<http://www.pleiadi.inaf.it>). FF acknowledges support from the INAF 2024 RSN1 Minigrant “The effect of a variable IMF on Galaxy Evolution and Assembly: from the local to the high- z Universe.” and from the Next Generation European Union PRIN 2022 “20225E4SY5 - From ProtoClusters to Clusters in one Gyr”. MH acknowledges funding from the Swiss National Science Foundation (SNSF) via a PRIMA grant PRO0P2-193577 ‘From cosmic dawn to high noon: the role of BHs for young galaxies’.

References

- Adams, N. J., Conselice, C. J., Austin, D., et al. 2024, *ApJ*, 965, 169
 Akins, H. B., Casey, C. M., Lambrides, E., et al. 2025, *ApJ*, 991, 37
 Álvarez-Márquez, J., Crespo Gómez, A., Colina, L., et al. 2025, *A&A*, 695, A250
 Álvarez-Márquez, J., Crespo Gómez, A., Colina, L., et al. 2023, *A&A*, 671, A105
 Arrabal Haro, P., Dickinson, M., Finkelstein, S. L., et al. 2023, *Nature*, 622, 707
 Baugh, C. M., Gonzalez-Perez, V., Lagos, C. D. P., et al. 2019, *MNRAS*, 483, 4922
 Bouwens, R. J., Oesch, P. A., Stefanon, M., et al. 2021, *AJ*, 162, 47
 Bruzual, G. & Charlot, S. 2003, *MNRAS*, 344, 1000
 Cameron, A. J., Katz, H., Witten, C., et al. 2024, *MNRAS*, 534, 523
 Cantarella, S., De Lucia, G., Fontanot, F., et al. 2025, *arXiv e-prints*, arXiv:2511.03787
 Cappellari, M., McDermid, R. M., Alatalo, K., et al. 2012, *Nature*, 484, 485
 Carnall, A. C., McLeod, D. J., McLure, R. J., et al. 2023, *MNRAS*, 520, 3974
 Carniani, S., Hainline, K., D’Eugenio, F., et al. 2024, *Nature*, 633, 318
 Casey, C. M., Akins, H. B., Shuntov, M., et al. 2024, *ApJ*, 965, 98
 Castellano, M., Fontana, A., Treu, T., et al. 2023, *ApJ*, 948, L14
 Chabrier, G. 2003, *ApJ*, 586, L133
 Charlot, S. & Fall, S. M. 2000, *ApJ*, 539, 718
 Chen, H., Xie, L., Wang, J., et al. 2024, *MNRAS*, 528, 2451
 Chieffi, A. & Limongi, M. 2002, *ApJ*, 577, 281
 Chon, S., Hosokawa, T., Omukai, K., & Schneider, R. 2024, *MNRAS*, 530, 2453
 Cueto, E. R., Hutter, A., Dayal, P., et al. 2024, *A&A*, 686, A138
 Cullen, F., Carnall, A. C., Scholte, D., et al. 2025, *MNRAS*, 540, 2176
 Curti, M., D’Eugenio, F., Carniani, S., et al. 2023, *MNRAS*, 518, 425
 Curti, M., Maiolino, R., Curtis-Lake, E., et al. 2024, *A&A*, 684, A75
 Curti, M., Witstok, J., Jakobsen, P., et al. 2025, *A&A*, 697, A89
 De Lucia, G., Fontanot, F., Xie, L., & Hirschmann, M. 2024, *A&A*, 687, A68
 De Lucia, G., Tornatore, L., Frenk, C. S., et al. 2014, *MNRAS*, 445, 970
 Dekel, A., Sarkar, K. C., Birnboim, Y., Mandelker, N., & Li, Z. 2023, *MNRAS*, 523, 3201

- Donnan, C. T., McLeod, D. J., Dunlop, J. S., et al. 2023, *MNRAS*, 518, 6011
- Donnan, C. T., McLure, R. J., Dunlop, J. S., et al. 2024, *MNRAS*, 533, 3222
- Dutton, A. A., Mendel, J. T., & Simard, L. 2012, *MNRAS*, 422, L33
- Euclid Collaboration, Scharré, L., Hirschmann, M., et al. 2024, *A&A*, 689, A276
- Finkelstein, S. L., Leung, G. C. K., Bagley, M. B., et al. 2024, *ApJ*, 969, L2
- Finkelstein, S. L., Ryan, Jr., R. E., Papovich, C., et al. 2015, *ApJ*, 810, 71
- Fiore, F., Ferrara, A., Bischetti, M., Feruglio, C., & Traverso, A. 2023, *ApJ*, 943, L27
- Fontanot, F. 2020, in *IAU Symposium*, Vol. 341, *Panchromatic Modelling with Next Generation Facilities*, ed. M. Boquien, E. Lusso, C. Gruppioni, & P. Tissera, 124–128
- Fontanot, F., Calabrò, A., Talia, M., et al. 2021, *MNRAS*, 504, 4481
- Fontanot, F., De Lucia, G., Hirschmann, M., et al. 2017, *MNRAS*, 464, 3812
- Fontanot, F., De Lucia, G., Hirschmann, M., et al. 2020, *MNRAS*, 496, 3943
- Fontanot, F., De Lucia, G., Xie, L., et al. 2025, *A&A*, 699, A108
- Fontanot, F., De Lucia, G., Xie, L., et al. 2018a, *MNRAS*, 475, 2467
- Fontanot, F., La Barbera, F., De Lucia, G., et al. 2024, *A&A*, 686, A302
- Fontanot, F., La Barbera, F., De Lucia, G., Pasquali, A., & Vazdekis, A. 2018b, *MNRAS*, 479, 5678
- Gallazzi, A. & Bell, E. F. 2009, *ApJS*, 185, 253
- Gallazzi, A., Charlot, S., Brinchmann, J., White, S. D. M., & Tremonti, C. A. 2005, *MNRAS*, 362, 41
- Gelli, V., Mason, C., & Hayward, C. C. 2024, *ApJ*, 975, 192
- González, V., Labbé, I., Bouwens, R. J., et al. 2011, *ApJ*, 735, L34
- Grazian, A., Fontana, A., Santini, P., et al. 2015, *A&A*, 575, A96
- Gunawardhana, M. L. P., Hopkins, A. M., Sharp, R. G., et al. 2011, *MNRAS*, 415, 1647
- Harikane, Y., Nakajima, K., Ouchi, M., et al. 2024, *ApJ*, 960, 56
- Harikane, Y., Ouchi, M., Oguri, M., et al. 2023a, *ApJS*, 265, 5
- Harikane, Y., Zhang, Y., Nakajima, K., et al. 2023b, *ApJ*, 959, 39
- Harvey, T., Conselice, C. J., Adams, N. J., et al. 2025, *ApJ*, 978, 89
- Hirano, S., Hosokawa, T., Yoshida, N., Omukai, K., & Yorke, H. W. 2015, *MNRAS*, 448, 568
- Hirschmann, M., De Lucia, G., & Fontanot, F. 2016, *MNRAS*, 461, 1760
- Hosokawa, T., Hirano, S., Kuiper, R., et al. 2016, *ApJ*, 824, 119
- Hutter, A., Cueto, E. R., Dayal, P., et al. 2025, *A&A*, 694, A254
- Jeřábková, T., Hasani Zonoozi, A., Kroupa, P., et al. 2018, *A&A*, 620, A39
- Katz, H., Rosdahl, J., Kimm, T., et al. 2022, *MNRAS*, 510, 5603
- Kocevski, D. D., Finkelstein, S. L., Barro, G., et al. 2025, *ApJ*, 986, 126
- Kokorev, V., Atek, H., Chisholm, J., et al. 2025, *ApJ*, 983, L22
- Kroupa, P. 2001, *MNRAS*, 322, 231
- Kroupa, P., Weidner, C., Pflamm-Altenburg, J., et al. 2013, *Planets, Stars and Stellar Systems. Volume 5: Galactic Structure and Stellar Populations*, 5, 115
- La Barbera, F., Ferreras, I., Vazdekis, A., et al. 2013, *MNRAS*, 433, 3017
- Labbé, I., van Dokkum, P., Nelson, E., et al. 2023, *Nature*, 616, 266
- Leitherer, C., Schaerer, D., Goldader, J. D., et al. 1999, *ApJS*, 123, 3
- Leung, G. C. K., Bagley, M. B., Finkelstein, S. L., et al. 2023, *ApJ*, 954, L46
- Li, Z., Dekel, A., Sarkar, K. C., et al. 2024, *A&A*, 690, A108
- Maio, U. & Péroux, C. 2026, *arXiv e-prints*, [arXiv:2603.00230](https://arxiv.org/abs/2603.00230)
- Maiolino, R., Scholtz, J., Curtis-Lake, E., et al. 2024, *A&A*, 691, A145
- Matthee, J., Naidu, R. P., Brammer, G., et al. 2024, *ApJ*, 963, 129
- Mattolini, D., Zibetti, S., Gallazzi, A. R., Scholz-Díaz, L., & Pratesi, J. 2025, *A&A*, 703, A5
- Mauerhofer, V., Dayal, P., Haehnelt, M. G., et al. 2025, *A&A*, 696, A157
- McLeod, D. J., Donnan, C. T., McLure, R. J., et al. 2024, *MNRAS*, 527, 5004
- Meng, J., Li, C., Mo, H. J., et al. 2023, *ApJ*, 944, 75
- Morishita, T., Stiavelli, M., Grillo, C., et al. 2024, *ApJ*, 971, 43
- Muratov, A. L., Kereš, D., Faucher-Giguère, C.-A., et al. 2015, *MNRAS*, 454, 2691
- Nakajima, K., Ouchi, M., Isobe, Y., et al. 2023, *ApJS*, 269, 33
- Navarro-Carrera, R., Rinaldi, P., Caputi, K. I., et al. 2024, *ApJ*, 961, 207
- Nomoto, K., Tominaga, N., Umeda, H., et al. 2005, *Nucl. Phys. A*, 758, 263
- Oke, J. B. & Gunn, J. E. 1983, *ApJ*, 266, 713
- Omukai, K. & Palla, F. 2003, *ApJ*, 589, 677
- Osman, O., De Lucia, G., Fontanot, F., Xie, L., & Hirschmann, M. 2025, *arXiv e-prints*, [arXiv:2512.15902](https://arxiv.org/abs/2512.15902)
- Papadopoulos, P. P., Thi, W.-F., Miniati, F., & Viti, S. 2011, *MNRAS*, 414, 1705
- Pérez-González, P. G., Costantin, L., Langeroodi, D., et al. 2023, *ApJ*, 951, L1
- Planck Collaboration XVI. 2014, *A&A*, 571, A16
- Robertson, B. E. 2022, *ARA&A*, 60, 121
- Sandage, A. 1986, *A&A*, 161, 89
- Sanders, R. L., Shapley, A. E., Topping, M. W., Reddy, N. A., & Brammer, G. B. 2023, *ApJ*, 955, 54
- Sanders, R. L., Shapley, A. E., Topping, M. W., Reddy, N. A., & Brammer, G. B. 2024, *ApJ*, 962, 24
- Semenov, V. A., Conroy, C., & Hernquist, L. 2025, *ApJ*, 989, 219
- Shuntov, M., Ilbert, O., Toft, S., et al. 2025, *A&A*, 695, A20
- Somerville, R. S., Popping, G., & Trager, S. C. 2015, *MNRAS*, 453, 4337
- Somerville, R. S., Yung, L. Y. A., Lancaster, L., et al. 2025, *MNRAS*[[arXiv:2505.05442](https://arxiv.org/abs/2505.05442)]
- Song, M., Finkelstein, S. L., Ashby, M. L. N., et al. 2016, *ApJ*, 825, 5
- Springel, V., White, S. D. M., Jenkins, A., et al. 2005, *Nature*, 435, 629
- Stefanon, M., Bouwens, R. J., Labbé, I., et al. 2021, *ApJ*, 922, 29
- Stefanon, M., Marchesini, D., Muzzin, A., et al. 2015, *ApJ*, 803, 11
- Taffoni, G., Becciani, U., Garilli, B., et al. 2020, *arXiv e-prints*, [arXiv:2002.01283](https://arxiv.org/abs/2002.01283)
- Tinsley, B. M. & Larson, R. B. 1979, *MNRAS*, 186, 503
- Trinca, A., Schneider, R., Valiante, R., et al. 2024, *MNRAS*, 529, 3563
- van Dokkum, P. G. & Conroy, C. 2024, *ApJ*, 973, L32
- van Dokkum, P. G. & Conroy, C. 2012, *ApJ*, 760, 70
- Vazdekis, A., Sánchez-Blázquez, P., Falcón-Barroso, J., et al. 2010, *MNRAS*, 404, 1639
- Weibel, A., Oesch, P. A., Barrufet, L., et al. 2024, *MNRAS*, 533, 1808
- Weidner, C., Kroupa, P., Pflamm-Altenburg, J., & Vazdekis, A. 2013, *MNRAS*, 436, 3309
- Whitler, L., Stark, D. P., Topping, M. W., et al. 2025, *arXiv e-prints*, [arXiv:2501.00984](https://arxiv.org/abs/2501.00984)
- Xie, L., De Lucia, G., Fontanot, F., et al. 2024, *ApJ*, 966, L2
- Xie, L., De Lucia, G., Hirschmann, M., & Fontanot, F. 2020, *MNRAS*, 498, 4327
- Xie, L., De Lucia, G., Hirschmann, M., Fontanot, F., & Zoldan, A. 2017, *MNRAS*, 469, 968
- Yung, L. Y. A., Somerville, R. S., Finkelstein, S. L., Wilkins, S. M., & Gardner, J. P. 2024, *MNRAS*, 527, 5929
- Yung, L. Y. A., Somerville, R. S., & Iyer, K. G. 2025, *MNRAS*[[arXiv:2504.18618](https://arxiv.org/abs/2504.18618)]
- Zibetti, S., Charlot, S., & Rix, H. 2009, *MNRAS*, 400, 1181
- Zibetti, S. & Gallazzi, A. R. 2022, *MNRAS*, 512, 1415
- Zibetti, S., Gallazzi, A. R., Ascasibar, Y., et al. 2017, *MNRAS*, 468, 1902
- Ziparo, F., Ferrara, A., Sommovigo, L., & Kohandel, M. 2023, *MNRAS*, 520, 2445

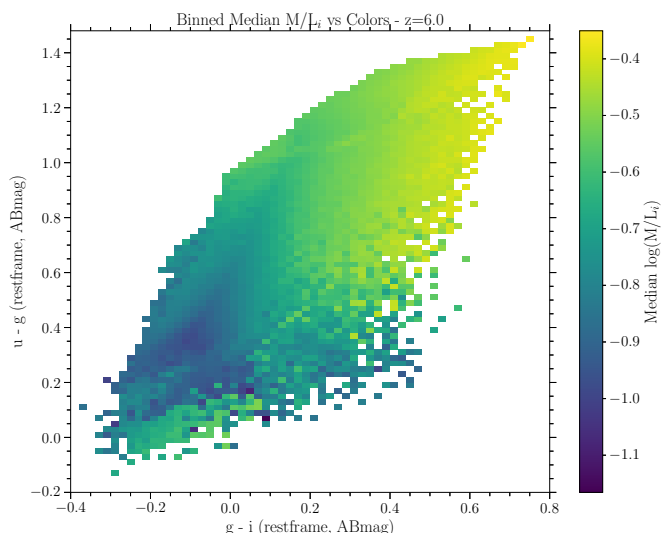


Fig. A.1. Stellar M/L in SDSS-*i* band (solar units) in the colour-colour space defined by $u - g$ versus $g - i$ (rest-frame SDSS filters, AB magnitudes), as it results by assuming a standard [Chabrier \(2003\)](#) IMF and the modelling described in the appendix text. The map represents the median M/L of the models in bins $0.02 \text{ mag} \times 0.02 \text{ mag}$ wide, according to the colorbar on the right. Only the 137,489 models with a SFH consistent with the age of the Universe at $z = 6$, i.e. $t_{\text{form,lb}} < 0.92 \text{ Gyr}$, are shown here. Note that the colours and the luminosities used for M/L computations are intrinsic, i.e. without any dust attenuation effect applied.

Appendix A: Stellar masses from optical rest-frame photometry

To simulate the stellar mass that an observer would infer from SED modelling based on standard stellar population assumptions and, in particular, a [Chabrier \(2003\)](#) IMF, we use the two-colour method introduced by ([Zibetti et al. 2009](#), ZCR09, hereafter). The idea is to build a vast library of composite SP models and express the M/L in a given band as a function of two optical colours, which capture the SED shape. Given a pair of “observed” colours from the simulations, the average M/L of the models in the corresponding small 2D colour bin is used to convert the observed luminosity into stellar mass.

Given the idealised nature of this experiment and to avoid folding uncertainties concerning the dust treatment into the colour dependence, we depart from ZCR09 by using models that include only pure stellar emission. The derived colours are consistently compared with the intrinsic stellar emission computed for the simulated galaxies.

The present library is based on the original SSP models of BC03, built on STELIB stellar templates and Padova 1994 evolutionary tracks. This choice ensures consistency with the SSPs used for the simulated galaxies. The composite SPs are built according to the SFH and chemical enrichment histories introduced by [Zibetti et al. \(2017\)](#). Each SFH includes a secular continuous component modelled as a delayed Gaussian function à la [Sandage \(1986\)](#), characterized by a lookback time for the beginning of the SFH ($t_{\text{form,lb}}$) and a timescale τ that corresponds to the time elapsed until the peak of the SFR is reached. These two parameters are randomly generated according to the following priors. For $t_{\text{form,lb}}$, we adopt a log-uniform prior between 500 Myr and the age of the Universe at the redshift of interest. Given $t_{\text{form,lb}}$, τ is generated from a log-uniform prior in $\tau/t_{\text{form,lb}}$ between 1/50 and 2. Random bursts are added following the pre-

descriptions of [Gallazzi et al. \(2005\)](#). Notably, our models implement a simple chemical evolution prescription, with a parameterization derived from leaky-box models, plus a randomization for the bursts. The allowed range of variation for the stellar metallicity is between 1/50 and $2.5 Z_{\odot}$ ($Z_{\odot} \equiv 0.02$). More details about the implementation of the bursts and of the chemical evolution are provided in Appendix A of [Mattolini et al. \(2025\)](#).

Fig. A.1 displays the variation of M/L in the SDSS *i* band (in solar units) across the plane defined by the optical colours $u - g$ versus $g - i$ (SDSS filters, AB system). Here we consider only models with $t_{\text{form,lb}} < 0.92 \text{ Gyr}$, corresponding to the age of the Universe at $z = 6$ (flat Λ CDM cosmology with $h = 0.7$, $\Omega_{\Lambda} = 0.7$).

The 137,489 models are binned in $0.02 \text{ mag} \times 0.02 \text{ mag}$ colour bins, and the median M/L in each bin is calculated and represented in the map. The resulting matrix is then linearly interpolated over the entries with no models and extended using a nearest-neighbour algorithm to the full colour-colour space. Each galaxy in the simulation is assigned the M/L of the corresponding colour-colour bin in this map. Note that the dispersion of M/L in each bin ranges between 0.05 and 0.15 dex, hence well below the typical mass excess determined in Fig. 5.

Note that by further restricting the maximum allowed $t_{\text{form,lb}}$ for higher z , the number of models decreases and the coverage of the space at the red end as well. However, we verified that such a more restrictive $t_{\text{form,lb}}$ selection does not significantly affect the M/L in the common colour-colour space. For this reason, we adopt the map for $z = 6$ as the reference look-up table for all redshifts.